

# Journal Pre-proof

Single-cell sequencing of peripheral blood mononuclear cells reveals distinct immune response landscapes of COVID-19 and influenza patients



Linnan Zhu, Penghui Yang, Yingze Zhao, Zhenkun Zhuang, Zhifeng Wang, Rui Song, Jie Zhang, Chuanyu Liu, Qianqian Gao, Qumiao Xu, Xiaoyu Wei, Hai-Xi Sun, Beiwei Ye, Yanan Wu, Ning Zhang, Guanglin Lei, Linxiang Yu, Jin Yan, Guanghao Diao, Fanping Meng, Changqing Bai, Panyong Mao, Yeya Yu, Mingyue Wang, Yue Yuan, Qiuting Deng, Ziyi Li, Yunting Huang, Guohai Hu, Yang Liu, Xiaoqian Wang, Ziqian Xu, Peipei Liu, Yuhai Bi, Yi Shi, Shaogeng Zhang, Zhihai Chen, Jian Wang, Xun Xu, Guizhen Wu, Fusheng Wang, George F. Gao, Longqi Liu, William J. Liu

PII: S1074-7613(20)30316-2

DOI: <https://doi.org/10.1016/j.immuni.2020.07.009>

Reference: IMMUNI 4417

To appear in: *Immunity*

Received Date: 29 April 2020

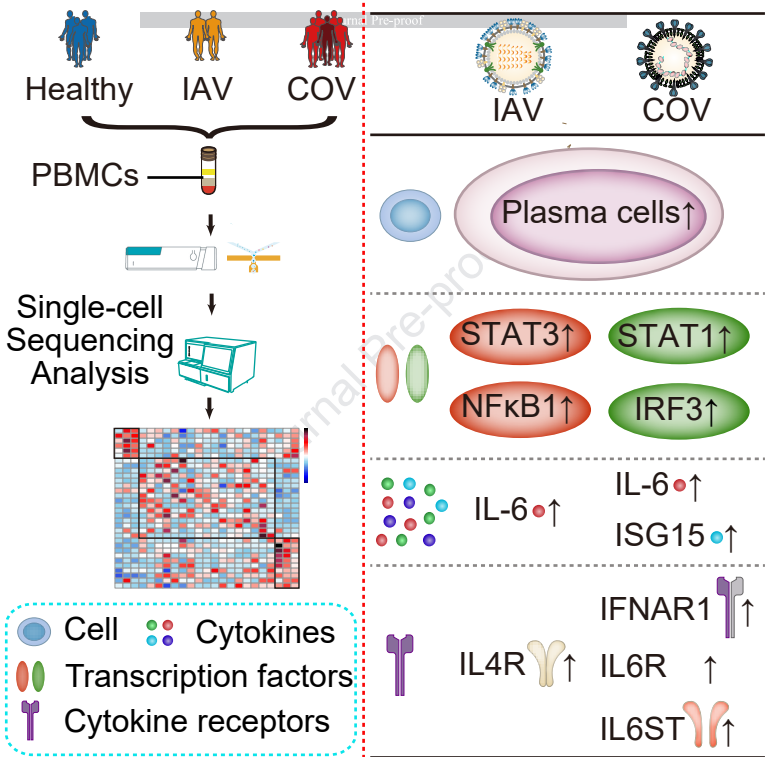
Revised Date: 7 June 2020

Accepted Date: 14 July 2020

Please cite this article as: Zhu, L., Yang, P., Zhao, Y., Zhuang, Z., Wang, Z., Song, R., Zhang, J., Liu, C., Gao, Q., Xu, Q., Wei, X., Sun, H.-X., Ye, B., Wu, Y., Zhang, N., Lei, G., Yu, L., Yan, J., Diao, G., Meng, F., Bai, C., Mao, P., Yu, Y., Wang, M., Yuan, Y., Deng, Q., Li, Z., Huang, Y., Hu, G., Liu, Y., Wang, X., Xu, Z., Liu, P., Bi, Y., Shi, Y., Zhang, S., Chen, Z., Wang, J., Xu, X., Wu, G., Wang, F., Gao, G.F., Liu, L., Liu, W.J., Single-cell sequencing of peripheral blood mononuclear cells reveals distinct immune response landscapes of COVID-19 and influenza patients, *Immunity* (2020), doi: <https://doi.org/10.1016/j.immuni.2020.07.009>.

This is a PDF file of an article that has undergone enhancements after acceptance, such as the addition of a cover page and metadata, and formatting for readability, but it is not yet the definitive version of record. This version will undergo additional copyediting, typesetting and review before it is published in its final form, but we are providing this version to give early visibility of the article. Please note that, during the production process, errors may be discovered which could affect the content, and all legal disclaimers that apply to the journal pertain.

© 2020 Published by Elsevier Inc.



1   **Single-cell sequencing of peripheral blood mononuclear cells**  
2   **reveals distinct immune response landscapes of COVID-19**  
3   **and influenza patients**

4

5   Linnan Zhu,<sup>1,2,11</sup> Penghui Yang,<sup>3,11</sup> Yingze Zhao,<sup>4,11</sup> Zhenkun Zhuang,<sup>1,2,6,11</sup> Zhifeng  
6   Wang,<sup>1,11</sup> Rui Song,<sup>5,11</sup> Jie Zhang,<sup>4,11</sup> Chuanyu Liu,<sup>1</sup> Qianqian Gao,<sup>1</sup> Qumiao Xu,<sup>1</sup>  
7   Xiaoyu Wei,<sup>1,8</sup> Hai-Xi Sun,<sup>1,2</sup> Beiwei Ye,<sup>4</sup> Yanan Wu,<sup>4</sup> Ning Zhang,<sup>7</sup> Guanglin Lei,<sup>3</sup>  
8   Linxiang Yu,<sup>3</sup> Jin Yan,<sup>3</sup> Guanghao Diao,<sup>3</sup> Fanping Meng,<sup>3</sup> Changqing Bai,<sup>3</sup> Panyong  
9   Mao,<sup>3</sup> Yeya Yu,<sup>1</sup> Mingyue Wang,<sup>1</sup> Yue Yuan,<sup>1</sup> Qiuting Deng,<sup>1</sup> Ziyi Li,<sup>1,9</sup> Yunting Huang,<sup>1</sup>  
10   Guohai Hu,<sup>1</sup> Yang Liu,<sup>1,8</sup> Xiaoqian Wang,<sup>1,10</sup> Ziqian Xu,<sup>4</sup> Peipei Liu,<sup>4</sup> Yuhai Bi,<sup>7</sup> Yi Shi,<sup>7</sup>  
11   Shaogeng Zhang,<sup>3</sup> Zhihai Chen,<sup>5</sup> Jian Wang,<sup>1,2</sup> Xun Xu,<sup>1,2</sup> Guizhen Wu,<sup>4</sup> Fusheng  
12   Wang,<sup>3\*</sup> George F. Gao<sup>4,7\*</sup> Longqi Liu,<sup>1,2\*</sup> William J. Liu,<sup>4,12\*</sup>

13

14   <sup>1</sup>BGI-Shenzhen, Shenzhen 518103, China;

15   <sup>2</sup>China National GeneBank, BGI-Shenzhen, Shenzhen 518120, China;

16   <sup>3</sup>The Fifth Medical Center of PLA General Hospital, National Clinical Research Center  
17   for Infectious Diseases, Beijing 100039, China;

18   <sup>4</sup>NHC Key Laboratory of Biosafety, National Institute for Viral Disease Control and  
19   Prevention, Chinese Center for Disease Control and Prevention, Beijing 102206,  
20   China;

21   <sup>5</sup>Center of Infectious Disease, Beijing Ditan Hospital, Capital Medical University,  
22   Beijing 100015, China;

23   <sup>6</sup>School of Biology and Biological Engineering, South China University of Technology,  
24   Guangzhou 510006, China;

25   <sup>7</sup>CAS Key Laboratory of Pathogenic Microbiology and Immunology, Institute of  
26   Microbiology, Chinese Academy of Sciences, Beijing 100101, China;

27   <sup>8</sup>BGI Education Center, University of Chinese Academy of Sciences, Shenzhen

28 518083, China;

29 <sup>9</sup> Northwest A & F University, Yangling, Shanxi 712100, China;

30 <sup>10</sup> BGI-Genolimmune, BGI-Shenzhen, Wuhan 4300794, China;

31 <sup>11</sup> These authors contributed equally;

32 <sup>12</sup> Lead Contact.

33

34

35 \* Correspondence: liujun@ivdc.chinacdc.cn (W.J.L.), liulongqi@genomics.cn (L.L.),

36 gaofu@chinacdc.cn (G.F.G.), fswang302@163.com (F.W.)

37 **Keywords:**

38 COVID-19, influenza, scRNA-seq, apoptosis, IL-6R

39

40 **SUMMARY**

41

42 COVID-19 is a severe infectious disease that is a current global health threat.  
43 However, little is known about its hallmarks compared to other infectious diseases.  
44 Here, we report the single-cell transcriptional landscape of longitudinally collected  
45 peripheral blood mononuclear cells (PBMCs) in both COVID-19 and influenza A virus  
46 (IAV)-infected patients. We observed increase of plasma cells in both COVID-19 and  
47 IAV patients, and XAF1-, TNF- and FAS-induced T cell apoptosis in COVID-19  
48 patients. Further analyses revealed distinct signaling pathways activated in COVID-19  
49 (STAT1 and IRF3) vs. IAV (STAT3 and NFkB) patients and substantial differences in  
50 the expression of key factors. These factors include relatively increase of *IL6R* and  
51 *IL6ST* expression in COVID-19 patients, but similarly increased IL-6 concentrations  
52 compared to IAV patients, supporting the clinical observations of increased  
53 pro-inflammatory cytokines in COVID-19 patients. Thus, we provide the landscape of  
54 PBMCs and unveil distinct immune response pathways in COVID-19 and IAV  
55 patients.

56

57 **INTRODUCTION**

58

59 A novel coronavirus (CoV), designated SARS-CoV-2, underlies a pandemic infection,

60 Corona Virus Disease 2019 (COVID-19), which rapidly spread globally and has been  
61 proclaimed as a severe public health emergency of international concern (PHEIC) by  
62 the World Health Organization (WHO) (Wang et al., 2020a). By June 30<sup>th</sup> 2020, more  
63 than 200 countries and territories reported COVID-19 infections, together comprising  
64 10,185,374 confirmed cases and 503,862 deaths (data from WHO, CDC, ECDC at  
65 <https://www.who.int/emergencies/diseases/novel-coronavirus-2019/situation-reports>).

66

67 Common respiratory viruses include CoV, influenza A virus (IAV), influenza B virus,  
68 respiratory syncytial virus, parainfluenza virus and adenovirus, etc. CoV belongs to  
69 the virus family *Coronaviridae*, which is an enveloped, nonsegmented, single  
70 stranded positive-sense RNA virus (Zhao et al., 2017). SARS-CoV-2 is a  
71 β-coronavirus, like middle east respiratory syndrome-coronavirus (MERS-CoV) and  
72 severe acute respiratory syndrome-coronavirus (SARS-CoV), all of which are  
73 suggested to have originated in bats (Zhou et al., 2020b). Evidence supports that the  
74 cellular receptor, angiotensin-converting enzyme 2 (ACE2), and the serine protease  
75 for SARS-CoV entry, transmembrane serine protease 2 (TMPRSS2) (Li et al., 2003),  
76 are key mediators for SARS-CoV-2 host cell entry (Wang et al., 2020b). It has been  
77 shown that ACE2 is expressed not only in the respiratory system, but in a range of  
78 organs, tissues and cell types (Xu et al., 2020a), indicating viral infection can rapidly  
79 spread throughout the body as disease progresses.

80

81 SARS-CoV first emerged in China in 2002-2003 and MERS-CoV was first reported in  
82 Saudi Arabia in 2012, with mortality rates around 10% (8,098 cases and 774 deaths,  
83 data from World Health Organization, WHO) and 34.4% (2,494 cases and 858 deaths,  
84 data from WHO) of SARS-CoV and MERS-CoV, respectively (Wu et al., 2020). In  
85 particular, based on the data collected from WHO (up to March 24<sup>th</sup>, 2020), 4.9% of  
86 SARS-CoV-2 cases are fatal (823,626 cases and 40,598 deaths), lower than that of  
87 MERS-CoV and SARS-CoV (Liu et al., 2017). Flu season occurs annually, and  
88 influenza symptoms are similar to respiratory diseases caused by coronaviruses.  
89 According to annual estimates of the burden of seasonal influenza in the United  
90 States, the influenza viruses have caused an estimated 9,200,000-35,600,000 million  
91 illnesses, 139,000-708,000 hospitalizations and 4,000-20,000 deaths from  
92 pneumonia & influenza and 12,000-56,000 deaths from respiratory & circulatory  
93 symptoms (data from 2010-2011 to 2015-2016 influenza seasons) with a mortality  
94 rate of 0.04%-0.83% (Rolfes et al., 2018).

95

96 SARS-CoV-2 infection diagnostics include pneumonia detection using computed  
97 tomographic (CT) scans and viral RNA detection (extracted and tested by real-time  
98 RT-PCR with SARS-CoV-2-specific primers and probes) in throat swab samples,  
99 secretions acquired from the lower respiratory tract, peripheral blood or feces.  
100 Patients with mild symptoms present with fever, cough, myalgia or fatigue, and  
101 sputum production, though infected individuals are sometimes asymptomatic. Such

102 mild symptoms rarely include intestinal signs and symptoms (Huang et al., 2020).

103

104 After COVID-19 diagnosis, other symptoms can be detected by routine blood  
105 examination. The neutrophils in 38% of COVID-19 patients were above the normal  
106 range, while the haemoglobin in 51% COVID-19 patients lies below the normal range,  
107 according to research at the Jinyintan Hospital in Wuhan, China. In addition,  
108 lymphocytes levels decreased in 35% of patients (Chen et al., 2020), suggesting  
109 possible dysfunctional cell-mediated immunity in COVID-19 patients.

110

111 In addition to acute respiratory distress syndrome (ARDS), virally driven  
112 hyperinflammation is another major cause of mortality (Huang et al., 2014). Increased  
113 proinflammatory cytokines or chemokines responses even initiated viral sepsis and  
114 overwhelming systemic inflammation, contributing to cytokine storm syndromes (CSS)  
115 that include acute inflammatory-induced lung injury and development of pneumonitis,  
116 ARDS and respiratory failure resulting in shock, hemodynamic instability, multiple  
117 organ dysfunction and even death. It has been reported that interleukin-6 (IL-6)  
118 concentrations and ferritin increase with illness deterioration in non-survivors  
119 compared with survivors within a subgroup of patients with COVID-19 (Zhou et al.,  
120 2020a). Furthermore, we recently reported that during the acute phase, a group of  
121 proinflammatory cytokines was up-regulated in lung injury (Murray score) in severe  
122 patients. Importantly, these cytokines can be used as biomarkers to predict disease

123 severity after SARS-CoV-2 infection (Liu et al., 2020).

124

125 Although there is accumulating clinical data regarding blood cell indices, underlying  
126 molecular mechanisms have yet to be clarified. Here, we report the transcriptome  
127 dynamics of peripheral blood mononuclear cells (PBMCs) from patients with  
128 COVID-19, comparing these to profiles in IAV patients and control, healthy donors.  
129 We examined the landscape and features of these infections by integrating single-cell  
130 RNA sequencing (scRNA-seq) with clinical symptoms. We observed an increased  
131 proportion of plasma cells, as well as a reduction of lymphocytes in the clinic. Further  
132 analyses suggest that XAF1-, TNF- and Fas-induced apoptosis may confer this  
133 reduction. Furthermore, distinct from IAV patients we found that expression of *IL6R*  
134 and *IL6ST* were up-regulated in COVID-19 patients, which synergistically promotes  
135 increased pro-inflammatory cytokines during pathogenesis. We also discovered that  
136 several interferon-stimulated genes (ISGs including *ISG15*, *IFI44*, *IFI44L* and *RSAD2*)  
137 were specifically up-regulated in PBMCs from COVID-19 patients, enhancing antiviral  
138 and immune modulatory functions after viral infection.

139

140 **RESULTS**

141

142 **Single-cell transcriptional landscape of PBMCs from COVID-19 and IAV patients**

143 To investigate the pathogenesis and mechanism of SARS-CoV-2 infections in  
144 COVID-19 patients, blood samples were collected from 3 healthy controls, 2  
145 IAV-infected patients and 5 COVID-19 patients including 4 patients (COV-1 to COV-4)  
146 with uncomplicated disease courses and 1 patient (COV-5) that subsequently  
147 progressed to severe disease (**Figure 1A and Table S1**). Seasonal IAV-infected  
148 patients were chosen as controls because both SARS-CoV-2 and IAV are contagious  
149 RNA viruses and both caused respiratory tract infection. However, COVID-19 has  
150 distinct clinical signatures compared to IAV infections including high morbidity and  
151 mortality. COVID-19 patients were enrolled within 5-10 days of symptom onset based  
152 on positive nucleic acid testing results, and the day when PBMCs were first collected  
153 was named day 1. Time points corresponding to disease onset and sample collection  
154 are listed in **Table S1**. PBMCs were also collected at subsequent time points as  
155 shown in **Figure 1A**. After filtering out cells with low quality, we obtained  
156 transcriptome data sets from 46,022 cells with an average of 2,000 cells for each  
157 participant at each time point (**Figure 1B**). To uncover immune cell populations in  
158 COVID-19, we performed unsupervised clustering and obtained 15 cell populations  
159 (**Figure 1C**). Immunocytes such as T cells, B cells, monocytes, NKs, DCs, stem cells  
160 and megakaryocytes were identified based on the expression of classic cell type  
161 markers (**Figure 1C**). With this approach, five populations were annotated as T cells  
162 including naïve T cells ( $CD3^+CCR7^+GZMA^-$ ), activated  $CD4^+$  T cells ( $CD3^+CD4^+IL7R^+$ ),  
163 cytotoxic  $CD8^+$  T cells ( $CD3^+CD8^+GZMA^+$ ), mucosal associated invariant T cells  
164 (MAIT cells) ( $CD3^+SLC4A10^+$ ) and cycling T cells ( $CD3^+MKI67^+$ ); four populations

165 were annotated as B cells including naïve B cells ( $MS4A1^+IGHG1^+$ ), plasma cells  
166 ( $MZB1^+IGHG1^+$ ), cycling plasma cells ( $MZB1^+IGHG1^+MKI67^+$ ) and memory B cells  
167 ( $MS4A1^+IGHG1^+$ ); two were annotated as NK cells ( $KLRF1^+$ ) and one population was  
168 labeled DCs ( $CD1C^+LYZ^+$ ) and monocytes ( $LYZ^+CD68^+$ ) (**Figures 1D and S1A**). Most  
169 of the clusters consisted of cells from multiple patients indicating common immune  
170 traits among patients. In addition, PBMC samples from patients did not express *ACE2*  
171 and *TMPRSS2* receptors and did not exhibit viral reads, indicating that SARS-CoV-2  
172 may not infect PBMCs (**Figure S1B**).

173

#### 174 **Increased plasma cells in PBMCs from COVID-19 and IAV patients**

175 The general patterns of PBMC cell populations were comparable across patients  
176 (**Figure 2A and Table S2**). The proportion of plasma cells and cycling plasma cells  
177 were increased significantly in both COVID-19 and IAV-infected patients (**Figures 2B**  
178 **and S2**), and there was no difference between these two types of virus infection. The  
179 increased plasma cells may induce protective neutralizing antibodies to prevent  
180 viruses infecting cells. As expected, when examining the functions of up-regulated  
181 genes in B cells of COVID-19 patients compared with healthy donors, protein complex  
182 assembly and protein transport-related pathways were especially enriched, which  
183 may be due to a large number of proteins are synthesized during this process (**Figure**  
184 **2C**). B cell activation-related pathways were also enriched (**Figure 2C**), and  
185 representative genes include *PRDM1*, *XBP1* and *IRF4* (**Figure 2D**). The identity and

186 function of plasma cells are dependent upon the transcription factors *PRDM1*, *XBP1*,  
187 and *IRF4* (Ochiai et al., 2013; Shaffer et al., 2004). *PRDM1* has a central role in  
188 determining and shaping the secretory arm of mature B cell differentiation and in  
189 promoting Ig synthesis. *XBP1* is a positively-acting transcription factor in the  
190 CREB-ATF family that is expressed at a high amounts in plasma cells, and is crucial  
191 for increasing protein synthesis in plasma cells (Shaffer et al., 2004). *IRF4* regulates  
192 immunoglobulin class switch recombination and sustained and higher concentrations  
193 of *IRF4* are known to promote the generation of plasma cells (Ochiai et al., 2013).  
194 Following increased plasma cells and expression of relevant transcription factors, we  
195 found that the expression of *CD2AP* on activated CD4<sup>+</sup> T cells was elevated  
196 compared with healthy controls (**Figure 2E**). The adaptor molecule *CD2AP* in CD4<sup>+</sup> T  
197 cells modulates the differentiation of follicular helper T cells, and improves protective  
198 antibody responses in viral infection (Raju et al., 2018). In addition to supporting  
199 plasma cell function, *TNFSF14* expression was also increased in activated CD4<sup>+</sup> T  
200 cells and cytotoxic CD8<sup>+</sup> T cells. These factors promote T cell activation as well as T  
201 cell recruitment to tissues from peripheral blood. *KDM5A*, which encodes an  
202 H3K4me3 demethylase that is required for NK cell and T cell activation, is  
203 up-regulated in NK cells and cytotoxic CD8<sup>+</sup> T cells of COVID-19 (**Figure 2E**). Taken  
204 together, these results demonstrated that elevated plasma cells and increased  
205 activation of T cells and NK cells in COVID-19 patients may contribute to defense  
206 against the virus.

207

208 **Interferon (IFN) response and lymphocyte apoptosis in COVID-19 patients**

209 Gene Ontology (GO) analyses were performed to gain insight into functions of  
210 different cell subsets between COVID-19 patients and healthy controls. Genes in the  
211 group “Response to type I interferon signaling” were enriched in T, B and NK cell  
212 subsets of D1 and D4, but not D16 samples (**Figures 3A and S3A**), consistent with  
213 the concept that the IFN response is essential to the response triggered by viral  
214 infection. Consistently, “Defense response to virus signaling” genes were also  
215 enriched in T, B, and NK cells of all five COVID-19 patients on D1 and D4, but not D16  
216 (**Figures 3A and S3A**) implying an ongoing immune response against SARS-CoV-2  
217 virus. Furthermore, endoplasm- and protein unfolding-related pathways were  
218 especially enriched in B cells at all the three time points (D1, D4, and D16) (**Figures**  
219 **3A and S3A**), which may be due to a higher proportion of plasma cells in B cell  
220 clusters because high demand of protein synthesis was required during antibody  
221 production. Other signaling pathways, such as “Regulation of chromosome  
222 organization”, “DNA conformation change”, etc. in SARS-CoV-2 infection were also  
223 upregulated. The roles of these genes will need further investigation.

224

225 Differential expressed genes (DEGs) in these transcriptomic profiles were then  
226 compared between COVID-19 patients and healthy controls. ISGs, which are vital to  
227 early viral control (Schoggins and Rice, 2011), were identified in patients infected with  
228 SARS-CoV-2 on D1 and D4 (**Figures 3B and S3B**), in line with the enrichment for

229 “Response to type I interferon signaling” pathways in our GO analysis (**Figures 3A**  
230 **and S3A**). Among these ISGs, *ISG15*, *IFI44L*, *MX1*, and *X-linked inhibitor of*  
231 *apoptosis (XIAP)-associated factor 1 (XAF1)* were up-regulated in T, B, NK, and DC  
232 cell subsets (**Figures 3B and S3B**). The expression of these four genes was also  
233 much higher in COVID-19 patients compared to healthy controls at the bulk level  
234 (**Figure 3C**). We then examined transcription dynamics of these genes during the  
235 disease process. To achieve this, we divided the disease processes of COVID-19  
236 patients from symptom onset to discharge into 4 stages (**Table S3**). We identified 6  
237 time-dependent expression patterns (**Figure 3D**) and investigated their biological  
238 significance (**Figure 3E**). Cluster 3 contain 158 genes that had decreased expression  
239 levels over time. The functions of these genes were significantly enriched in biological  
240 processes associated with interferon responses, indicating that the transcriptional  
241 regulation of these genes is dynamic, and that they were activated at early time points  
242 and deactivated at late time points (**Figure 3E**). Cluster 1 contains 38 genes whose  
243 expression levels were elevated from stage 2. GO enrichment analysis showed that  
244 their functions were significantly enriched in translation and protein synthesis-related  
245 pathways. This is consistent with the timing of antibody production (Thevarajan et al.,  
246 2020), since a large amount of proteins synthesis occurs during this process (**Figure**  
247 **3E**).

248

249 Severe patient (COV-5) had a stronger response to interferons upon SARS-CoV-2

250 infection than the mild patients. In addition, the expression of *ISG15*, *IFI44L*, *MX1*,  
251 and *XAF1* was higher at earlier time points of disease progression, and then  
252 decreased at later phases individually (**Figure S3C**), illustrating their dynamic  
253 responses to interferons.

254

255 The ubiquitin-like protein ISG15, IFI44L and MX1 all have roles in the antiviral  
256 response (Perng and Lenschow, 2018), while XAF1 participates in pro-apoptotic  
257 responses and has been reported to form a positive feedback loop with IRF-1 that  
258 drives apoptosis under stress (Jeong et al., 2018). TP53-mediated apoptosis was also  
259 enhanced by XAF1 via post-translational modification (Zou et al., 2012).Therefore,  
260 expression of genes linked to XAF1-mediated apoptosis, including *IRF1*, *TP53*,  
261 *BCL2L11* and *CASP3*, was analyzed (**Figure S3D**). Expression of *IRF1*, *TP53*, and  
262 *CASP3* was increased in T, B and NK cell subsets in COVID-19 patients compared to  
263 controls, while *BCL2L11* exhibited different patterns in different cell subsets. In  
264 addition to the XAF1 related apoptosis pathway, expression of genes in other  
265 apoptosis-linked pathways, including TNF- and Fas pathways (Elmore, 2007), was  
266 examined in both COVID-19 patients and healthy controls (**Figures 3F and S3E**). The  
267 expression of *TNFSF10* (*TRAIL*) and its receptor *TNFRSF10A* were increased in T  
268 cells from COVID-19 patients relative to healthy controls. Other TNF path member,  
269 including *TNFRSF1B*, were also relatively up-regulated in COVID-19 patients. As for  
270 the FAS path, the expression of *FAS*, *FASLG*, and *FADD* were up-regulated in T cells

271 of COVID-19 patients, though not significantly (**Figure 3F**). In B and NK cell subsets,  
272 *TNFSF10* and *FADD* were notably increased in COVID-19 patients with other genes  
273 increased mildly, except that *Fas* in B cells and *TRADD* in NK cells were subtly  
274 decreased (**Figure S3E**). Taken together, we find that up-regulated genes relevant to  
275 the XAF1-, TNF-, and Fas pathways may lead to increased T cell apoptosis in  
276 COVID-19 patients.

277

#### 278 **Immune molecular signatures of COVID-19 patients compared to IAV patients**

279 Next, we sought to identify the immune molecular signatures associated with  
280 COVID-19 and IAV infection. Thus, we compared the expression of cytokines,  
281 cytokine receptors and transcription factors in T cell subsets, NK cells and DCs  
282 among COVID-19 patients, IAV patients and healthy controls (**Figures 4A and S4A**).  
283 As the gene clustering pattern suggested, up-regulated genes in COVID-19 patients  
284 mostly encode proinflammatory cytokines, cytokine receptors and  
285 interferon-responsive transcription factors, while in IAV patients, proinflammatory  
286 transcription factors and virus-interacting host factors seem to be highly expressed.

287

288 Multiple key transcription factors involved in the host immune response, including  
289 *STAT3*, *NFKB1*, *REL* were up-regulated in various cell types from IAV patients  
290 (**Figures 4A and S4A**). *NFKB1* and *REL* encode active subunits of NF-κB  
291 heterodimer, one of the hallmark transcription factors activated by IAV infection  
14

292 (Ludwig and Planz, 2008). Activation of NF- $\kappa$ B plays a key role in regulating the  
293 proinflammatory innate immune response and adaptive immune response. Previous  
294 work showed that IL-6 and IL-10 are highly increased in severe IAV patients (Yu et al.,  
295 2011), known activators of STAT3 signaling. Expression of *STAT3* was elevated in IAV  
296 patients compared to COVID-19 patients and healthy controls, and seemed to  
297 correlate with time post-admission. In addition, *RUNX3* expression was up-regulated  
298 in activated CD4 $^{+}$  T cells of IAV patients compared to the other groups (**Figure 4B**). It  
299 has been suggested that RUNX3 induction is a key step for CD4 $^{+}$  T cells to acquire  
300 cytotoxic activity, whereas another study showed that RUNX3 induced by IAV  
301 infection through the NF- $\kappa$ B pathway promoted apoptosis in airway epithelial cells  
302 (Gan et al., 2015). The role of RUNX3 in the T cell-mediated immune response  
303 remains to be determined. Several pro-viral host factors such as *CHD1*, *BCLAF1*, and  
304 *PHF3* that contribute to viral infection, replication and immune evasion, were also  
305 up-regulated in IAV patients (**Figures 4A and S4A**) (Shapira et al., 2009). To see how  
306 response of these genes changes over time, we divided the disease processes of IAV  
307 patients into 2 stages (**Table S3**). We did not find any gene exhibiting statistically  
308 significant time-dependent regulation, although some them had trends toward  
309 increased or decreased expression (**Figures S4B and S4C**).

310

311 For COVID-19 patients, STAT1, a major transcription factor activated in response to  
312 interferon, was up-regulated in activated CD4 $^{+}$  T cells, cytotoxic CD8 $^{+}$  T cells, naïve T

313 cells and DCs (**Figures 4A and S4A**). Several proinflammatory factors, including TNF  
314 and TNFSF14, were elevated in activated CD4<sup>+</sup> T cells, cytotoxic CD8<sup>+</sup> T cells, MAIT  
315 cells, and NK cells (**Figures S4A and S4E**), suggesting enhanced effector function  
316 and memory cell development (Desai et al., 2018). Expression of *IL6* was not  
317 detectable in PBMCs of all patients or healthy controls. We measured plasma  
318 concentrations of IL-6 during hospitalization of these COVID-19 patients and after  
319 leaving the hospital (**Figure S4D**). Plasma IL-6 were above the normal range (0.0-7.0  
320 pg/mL) (Chen et al., 2020) in 2 out of 5 patients when admitted to the hospital,  
321 dropped back to normal during hospitalization, and remained stable after recovery.  
322 There was a rising phase of IL-6 in most COVID-19 patients indicating an active  
323 inflammatory response, which is also observed in IAV patients (Yu et al., 2011). The  
324 patient with severe symptoms had a much higher level of IL-6 when hospitalized, and  
325 it took longer to return to normal plasma IL-6 levels, which corresponded to disease  
326 severity.

327

328 IL-6 exerts its function by binding to IL-6R. The IL-6-IL-6R complex then binds to  
329 GP130 (Interleukin-6 receptor subunit beta, IL6ST), a common signal-transducing  
330 chain shared by several related cytokines (Mihara et al., 2012). Expression of *IL6R*  
331 was elevated in activated CD4<sup>+</sup> T cells, naïve T cells and DCs of COVID-19 patients  
332 compared to IAV patients and healthy controls (**Figures 4C and S4A**). Meanwhile,  
333 expression of *IL6ST* was up-regulated in various cell types from COVID-19 patients

334 and IAV patients compared to healthy controls . It has been reported that IL-6R is  
335 often shed from the membrane of activated T cells whereupon it binds the soluble  
336 form of IL-6 and acts *in trans* upon cells expressing IL6ST. Such IL-6 trans-signaling  
337 via IL6ST may contribute significantly to the proinflammatory properties of IL-6 (Wolf  
338 et al., 2014), emphasizing the potential importance of *IL6ST* upregulation observed in  
339 the current study.

340

341 Based on clinical observations that plasma concentrations of inflammatory cytokines,  
342 such as IFN- $\alpha$ 2, IL-7, IL-17, and IL-10 were higher in COVID-19 patients than in  
343 healthy adults (Huang et al., 2020), we compared expression levels of their  
344 corresponding receptors in activated CD4 $^{+}$  T cells, cytotoxic CD8 $^{+}$  T cells, MAIT cells,  
345 and NK cells across COVID-19 patients, IAV patients and healthy controls. (**Figure**  
346 **S4E**). Upregulation of IFNAR1, the alpha chain of the interferon  $\alpha/\beta$  receptor, was  
347 significant in these cell types in COVID-19 patients compared to healthy controls.  
348 Notably, along with IFNAR1, receptor subunits for IL-7, IL-17, IL-27 were substantially  
349 elevated in activated CD4 $^{+}$  T cells of COVID-19 patients compared to other groups,  
350 indicating that CD4 $^{+}$  T cells might be involved in major inflammatory response to  
351 cytokines.

352

353 Finally, we examined temporal changes in their expression (**Figures S4B and S4C**).  
354 Although some interferon-responsive transcription factor genes, such as *STAT1* and

355 *IRF3*, tend to have decreased expression levels over time, none of these patterns  
356 were statistically significant due to the limited number of patients. Future studies with  
357 more patients and more time points will address this question.

358

359 **DISCUSSION**

360

361 Emerging and re-emerging viruses pose a continuous threat to human health (Gao,  
362 2018). The new SARS-CoV-2 virus infection causes severe pulmonary disease and  
363 complications with significant morbidities and mortalities. Currently, there is no optimal  
364 treatment or effective drug for this fatal lung disease. Our current understanding of the  
365 host immune response to SARS-CoV-2 infection is limited, making it difficult to design  
366 urgently needed novel therapeutics. Here, we performed single-cell RNA sequencing  
367 on PBMCs from COVID-19 patients. Overall, the infection of SARS-CoV-2 has little  
368 impact on the composition of immune cells in PBMC. Among all the immune cell  
369 clusters, the percentage of plasma cells was increased significantly among all five  
370 COVID-19 patients compared with healthy controls. This increase in plasma cells  
371 could produce multiple protective neutralizing antibodies. These B cell-derived  
372 antibodies generated in response to SARS-CoV-2 are critical for preventing death  
373 from acute respiratory tract infections and providing continued protection from future  
374 infection-induced illness and/or death. In addition, blood plasma containing protective  
375 neutralizing antibodies from recovered patients is currently being encouraged for use

376 to treat severely affected patients.

377

378 IFN can be induced by viral infection to exert antiviral functions and balance virus  
379 control and immune pathology during this process. In SARS-CoV-2-infected ICU  
380 patients, plasma IFNy and TNF $\alpha$  levels were higher (Huang et al., 2020). IFN $\alpha$ 2 and  
381 IFNy have also been strongly associated with lung injury in COVID-19 (Liu et al.,  
382 2020). In addition, IFNy and GM-CSF co-expressing Th1 cells were only found in ICU  
383 patients infected by SARS-CoV-2 compared to healthy controls (Zhou et al., 2020c).

384 Consistently, “IFN-I response” was enriched in different PBMC cell subsets of  
385 COVID-19 patients in our study. Furthermore, expression of ISGs including *ISG15*,  
386 *IFI44L*, *MX1*, and *XAF1* was significantly up-regulated in these patients compared to  
387 three healthy controls, indicating that strong antiviral functions by interferons may be  
388 triggered (Perng and Lenschow, 2018). Moreover, severe COVID-19 patients showed  
389 a stronger response to interferons and virus infection compared to mild patients and  
390 healthy ones. This indicates that the intensity of the interferon response may indicate  
391 both the severity of COVID-19 disease, and distinguish COVID-19 patients from  
392 healthy individuals. Additionally, the dynamics of the interferon response suggest the  
393 individual differences and indicate that the timing of IFN therapy against SARS-CoV-2  
394 infection is critical.

395

396 According to our results, up-regulated *XAF1* expression may be involved in increased

397 T cell apoptosis in COVID-19 patients, cooperating with other genes including *IRF1*,  
398 *TP53*, *BCL2L11*, and *CASP3* (Jeong et al., 2018; Zou et al., 2012). Consistently, *TP53*  
399 expression was increased in COVID-19 patients in another COVID-19 study (Xiong et  
400 al., 2020). In addition to XAF1-induced apoptosis, the extrinsic pathway of apoptosis,  
401 including TNF- $\alpha$ /TNFR1 and Fas/FasL path (Elmore, 2007) were also found to be  
402 involved in different cell subtypes in COVID-19 patients. Moreover, plasma TNF $\alpha$  was  
403 reported to be increased in severe cases of COVID-19 (Chen et al., 2020; Huang et  
404 al., 2020) and TNF expression was up-regulated in PBMCs of COVID-19 patients in  
405 our study, demonstrating a correlation between increased TNF $\alpha$  secretion and  
406 TNF $\alpha$ -induced apoptosis in COVID-19 patients (Rath and Aggarwal, 1999). XAF1 can  
407 be induced by TNF $\alpha$  as well as IFN, and functions as an alternative pathway for  
408 TNF $\alpha$ -induced apoptosis (Straszewski-Chavez et al., 2007). XAF1 was also reported  
409 to collaborate with TNFSF10 (TRAIL) to promote Dengue virus-induced apoptosis  
410 (Zhang et al., 2019). Taken together, we found that the up-regulated genes relevant to  
411 XAF1-, TNF-, and Fas pathways may lead to increased T cell apoptosis in COVID-19  
412 patients.

413

414 We analyzed the expression of cytokines, cytokines receptors and transcription  
415 factors that are essential in the immune responses to viral infection, and pinpointed  
416 gene expression patterns in COVID-19 patients that differ from IAV patients. The  
417 up-regulation of cytokine receptors was in accordance with increased serum cytokine

418 levels, which might enhance the cytokine-mediated inflammatory responses. The fact  
419 that expression of most cytokines was not detected in PBMCs might indicate that  
420 serum cytokines largely arise from the infection site, i.e. the lower respiratory tract for  
421 COVID-19. We found that plasma concentrations of IL-6 are above normal levels in  
422 the majority of COVID-19 patients, consistent with other studies (Chen et al., 2020).  
423 Elevated IL-6 was also reported in IAV patients (Yu et al., 2011) and it is an immune  
424 signature in patients with acute respiratory stress syndrome (Wang et al., 2020c)  
425 which is associated with mortality caused by cytokine release syndrome. Currently,  
426 treatments blocking IL-6 or IL-6R have been approved for patients with pneumonia  
427 and elevated IL-6 , and a small-sized study has demonstrated the efficacy of  
428 Tocilizumab, a monoclonal antibody against IL-6R, in alleviating clinical symptoms (Xu  
429 et al., 2020b). Our data show that expression of *IL6R* and *IL6ST* was up-regulated in  
430 patients with COVID-19, and we suggest that increased expression of *IL6R* and *IL6ST*  
431 might synergize with elevated IL-6 to induce a strong inflammatory response,  
432 indicating that patients might benefit from IL-6 or IL-6R antagonist treatment.

433

#### 434 **Limitations of the study**

435 There are important limitations to the interpretation of this study. First, because only a  
436 limited number of patients were examined in our study, especially for IAV (2 patients),  
437 the differences between COVID-19 and IAV during infection we identified need to be  
438 further validated by larger clinical trials and/or by further studies. Second, our study

439 focuses on the single-cell transcriptome of PBMCs in blood. If we can combine our  
440 data with data from lesion sites such as the lung, our analysis will be more systematic  
441 and thus the conclusions would be more comprehensive.

442

443 Together, our study visualized the dynamic landscape of immune responses during  
444 the disease process in COVID-19 patients compared to IAV patients at the single-cell  
445 transcriptome level. These results not only represent the immune molecular and  
446 cellular signatures during the clinical process of COVID-19, but also suggest avenues  
447 to both diagnostic biomarkers and therapeutic targets, urgently needed for this novel  
448 disease.

449

450 **ACKNOWLEDGMENTS**

451 We thank Yuxuan Liu (BGI) and Bo Li (BGI) for assisting the single-cell RNA-seq  
452 library preparation. We also thank Dr. Andres Keller (Saarland University, Germany)  
453 for helpful discussion and evaluation of the DNBelab C4 technology. The study was  
454 supported by CAMS Research Units of Adaptive Evolution and Control of Emerging  
455 Viruses (2018RU009), National Mega-projects for Infectious Diseases  
456 (2020ZX10001016-005-001) and Beijing New-star Plan of Science and Technology  
457 (Z181100006218080). William J. Liu is supported by the Excellent Young Scientist  
458 Program of the National Natural Science Foundation of China (NSFC, 81822040) and  
459 the National Youth Talent Support Program. The study was supported by the National  
22

460 Natural Science Foundation of China (grants 81971564), the Science, Technology  
461 and Innovation Commission of Shenzhen Municipality (JSGG20180508152912700)  
462 and Shenzhen Key Laboratory of Single-Cell Omics (ZDSYS20190902093613831).

463 Editing support was received from Life Sciences Editors.

464

465 **AUTHOR CONTRIBUTIONS**

466 W.J.L., L.L., G.F.G., and F.W. designed and supervised the study. W.J.L., L.L. and G.F.G.  
467 conceived the project. J.G., J.L., J.P., C.B., Mei Z., H.X., G.Q., X.H., P.Y., Y.Z., R.S.,  
468 N.Z., G.L., L.Y., J.Y., X.W., Y.L., B.L. and G.D. collected clinical samples and analyzed  
469 the clinical and treatment data. Z.W., C.L., Y.Y., M.W., Y.Y., Q.D., Y.W., G.H., Y.Z., B.Y.,  
470 and J.Z. performed the experiments. L.Z., Z.Z., Q.G., Q.X., X.W., H.-X.S., L.L., Y.Z.,  
471 L.L. and W.J.L. analyzed the data. P.L., Y.B., Y.S., G.W., and Z.C. contributed to  
472 fruitful discussions and key ideas. L.Z., Q.G., Q.X., H.-X.S., Z.L., L.L., Y.Z., W.J.L., F.W.,  
473 and G.F.G. wrote the manuscript. J.W., X.X., L.L., Y.Z., W.J.L. and G.F.G. participated  
474 in the manuscript editing and discussion.

475

476 **DECLARATION OF INTERESTS**

477 Employees of BGI have stock holdings in BGI.

478

479 **Figure 1. Single-cell gene expression profiling of immune cells derived from**

480 **PBMCs.**

481 (A) Schematic outline of the study design. Ten subjects including 3 healthy donors, 5

482 COVID-19 patients, and 2 IAV-infected patients were included in this study.

483 (B) Bar plot shows the  $\log_{10}$  transformed cell number of each sample for every donor

484 at different time points. Blue represents 3 healthy donors, orange represents 2

485 IAV-infected patients and 5 COVID-19 patients are displayed using 5 different colors.

486 (C) The clustering result of 46,022 cells from 10 donors. Each point represents one

487 single cell, colored according to cell type. "Mega." is short for Megakaryocytes.

488 (D) Expression levels of cell typing genes in cell type clusters. CD3G for T cells,

489 KLRF1 and XCL1 for NKs, MS4A1 for B cells, IGHG1 and MZB1 for Plasma cells,

490 CD68 for Monocytes, LYZ for DCs, MKI67 and TOP2A for Cycling T cells, GZMA for

491 Cytotoxic CD8<sup>+</sup> T cells and NKs, PPBP for Megakaryocytes.

492 See also Figure S1 and Table S1.

493

494 **Figure 2. Dynamic composition and functional changes in immune cells during**

495 **SARS-CoV-2 infection.**

496 (A) The cell type frequency in each sample. Bars are colored by cell types.

497 (B) Differences in Plasma and Cycling Plasma proportion among samples from

498 healthy donors (Ctrl) (n=3), COV-19 patients (COV) (n=16), IAV patients (IAV) (n=4).

499 Student's t test was applied to test the significance of the difference. \* p<0.05,  
500 \*\*p<0.01, \*\*\*p<0.001.

501 (C) Enriched GO terms for upregulated genes in COVID-19 patients compared to  
502 healthy controls in B cells.

503 (D) The differential expression levels of B cell activation related genes *PRDM1*, *XBP1*  
504 and *IRF4* between healthy donors (Ctrl) and COVID-19 patients (COV) in plasma cells.

505 (E) The expression levels of T cell activation related genes in activated CD4<sup>+</sup> T cells,  
506 Cytotoxic CD8<sup>+</sup> T cells and NKs in samples from healthy donors and COVID-19  
507 patients. In the upper panel, the color of each dot represents expression levels of the  
508 gene, while the dot size represents the fraction of cells expressing the gene in the  
509 specific cell type. In the lower panel, the difference between healthy donors (Ctrl) (n=3)  
510 and COVID-19 patients (COV) (n=16) were tested using the student's t test. \* p<0.05,  
511 \*\*p<0.01, \*\*\*p<0.001.

512 See also Figure S2 and Table S2.

513

514 **Figure 3. Analysis of IFN response and apoptosis-associated genes in**  
515 **COVID-19 patients.**

516 (A) The top 20 enriched biological processes by Gene Ontology analysis in Day 1  
517 samples from COVID-19 patients, compared to healthy controls in different cell  
518 populations. Dot color indicates the statistical significance of the enrichment (*P* value)

519 and dot size represents gene ratio annotated to each term.

520 (B) The differentially expressed genes in Day1 samples from COVID-19 patients  
521 compared to healthy controls in different cell subsets. Red dots represent genes  
522 upregulated in COVID-19 patients (adjusted P-value < 0.01 and FC >= 2) while blue  
523 dots represents downregulated genes in COVID-19 patients (adjusted P-value < 0.01  
524 and FC <= 0.5). Genes with  $\log_2(\text{FC}) \geq 1.5$  were labeled by gene symbols.

525 (C) The gene expression of *ISG15*, *IFI44L*, *MX1*, and *XAF1* in healthy donors (Ctrl)  
526 (n=3) and COVID-19 patients (COV) (n=16). Student's t test was applied to test the  
527 significance of the difference. \* p<0.05, \*\*p<0.01, \*\*\*p<0.001.

528 (D) Genes clustered by their expression pattern along the progression of the disease  
529 by the mfuzz R package.

530 (E) The top10 enriched biological processes in each cluster of genes, as revealed by  
531 Gene Ontology analysis.

532 (F) The difference in expression levels of apoptosis-associated genes between  
533 COVID-19 patients (COV) (n=5) and healthy controls (Ctrl) (n=3) in T cells. Student's t  
534 test was applied. \* p<0.05, \*\*p<0.01, \*\*\*p<0.001.

535 See also Figure S3 and Table S3.

536

537 **Figure 4. Hallmarks of COVID-19 compared to IVA (revealed by single-cell**  
538 **analysis of cytokines, cytokine receptors and transcription factors).**

539 (A) The relative expression level (Z-score) of key cytokines, cytokine receptors and  
540 transcription factors among COVID-19 patients, IVA patients and healthy controls in  
541 the activated CD4<sup>+</sup> T cells population.

542 (B) The expression level of 4 representative genes highly expressed in activated  
543 CD4<sup>+</sup> T cells of IVA patients. Upper panel: the color of each dot in the dot plot  
544 indicates expression level of the gene; dot size represents the fraction of cells  
545 expressing the gene in activated CD4<sup>+</sup> T cells population. Lower panel: difference in  
546 gene expression among samples from COVID-19 patients (COV) (n=16), IVA patients  
547 (IAV) (n=4) and healthy donors (Ctrl) (n=3). Each dot in the box plot represents the  
548 average expression level of a gene in the activated CD4<sup>+</sup> T cells population in one  
549 sample. Student's t test was applied to test the significance of the difference. \* p<0.05,  
550 \*\*p<0.01, \*\*\*p<0.001. (C) Similar to panel B, showing 4 representative genes highly  
551 expressed in the activated CD4<sup>+</sup> T cells of COVID-19 patients.

552 See also Figure S4.

553

554 **STAR METHODS**

555 **RESOURCE AVAILABILITY**

556 **Lead Contact**

557 Further information and requests for resources and reagents should be directed to  
558 and will be fulfilled by the Lead Contact, William Jun Liu ([liujun@ivdc.chinacdc.cn](mailto:liujun@ivdc.chinacdc.cn))

559

560 **Materials Availability**

561 All unique reagents generated in this study are available from the Lead Contact  
562 without restriction.

563

564 **Data and Code Availability**

565 Raw and processed data are available on CNGB Nucleotide Sequence Archive  
566 (CNSA:<https://db.cngb.org/cnsa>) with accession number CNP0001102. The code  
567 supporting the current study are available from the corresponding author on request.

568

569 **EXPERIMENTAL MODEL AND SUBJECT DETAILS**

570 Five patients with COVID-19 were recruited in the Fifth Medical Center of PLA  
571 General Hospital from January to February 2020. Patients were divided into mild and  
572 severe groups according to the Fifth Revised Trial Version of the Novel Coronavirus  
573 Pneumonia Diagnosis and Treatment Guidance. Influenza virus infection, Respiratory  
574 syncytial virus infection and adenovirus infection were excluded in all patients with  
575 COVID-19. Two patients with IAV were collected in the Beijing Ditan Hospital, Capital  
576 Medical University from January to February 2018. Two Patients with IAV were  
577 diagnosed as having severe infection. The clinical characteristics of these patients are  
578 provided in **Tables S1 and S2**.

579

580 **METHOD DETAILS**

581 **Ethics statement**

582 The study was approved by the Ethics Committee of the Fifth Medical Center of PLA  
583 General Hospital and Beijing Ditan Hospital, Capital Medical University. Written  
584 informed consent was obtained from all participants (including one from a teenager's  
585 parents).

586

587 **Clinical information**

588 Throat swab and blood samples were collected from patients at various time-points  
589 after hospitalization. Sample collection, processing, and laboratory testing complied  
590 with WHO guidance. Viral RNA was extracted from throat swabs using the QIAamp  
591 Viral RNA Mini Kit (Qiagen) according to the manufacturer's instructions.  
592 SARS-CoV-2-infected patients were confirmed using the Novel Coronavirus  
593 (SARS-CoV-2) Nucleic Acid Detection kit (BioGerm).

594

595 All clinical information including demographic data, medical history, symptoms, signs,  
596 and laboratory data were collected from patient medical records. Laboratory data,  
597 included blood routine, lymphocyte subsets, infection-related biomarkers,  
598 inflammatory cytokines. The total number of leukocytes, percentage of neutrophils  
29

599 and percentage of lymphocytes in peripheral blood were counted by hemocytometer.  
600 The number and percentage of lymphocyte subsets was analyzed using the  
601 FACSCanto flow cytometer for COVID-19 patients on admission. C-reactive protein  
602 and Lactic acid was detected by the Beckman automatic biochemical analyzer.  
603 Interleukin 6 (IL-6) was detected using the ROCHE Elecsys IL-6 assay.

604

605 **Peripheral blood mononuclear cell (PBMC) collection**

606 PBMCs were isolated from heparinized venous blood of COVID-19 patients or healthy  
607 donors using a FicollR Paque Plus (Sigma Aldrich) solution according to standard  
608 density gradient centrifugation methods. Cells were harvested and counted via  
609 Cellaca MX high-throughput cell counter (Nexcelom Bioscience). The PBMCs were  
610 resuspended in 90% FBS, 10% DMSO freezing media and frozen using a Nalgene®  
611 Mr. Frosty® Cryo 1°C Freezing Container (Thermo Fisher Scientific) in a -80°C  
612 freezer for 24 hours before being transferred to liquid nitrogen for long-term storage.

613

614 **Single-cell suspension preparation**

615 Frozen vials of PBMCs were rapidly thawed in a 37°C water bath for ~2 minutes, and  
616 the vials were removed when a tiny ice crystal was left. Thawed PBMCs were  
617 quenched with 4 ml 37°C pre-warmed 1X phosphate-buffered saline (PBS, Thermo  
618 Fisher Scientific) and supplemented with 10% fetal bovine serum (FBS, HyClone).

619 Cells were centrifuged at 500 x g for 10 minutes at room temperature each time. The  
620 supernatant was removed, and the cell pellet was resuspended in 3 ml 1X PBS  
621 containing 0.04% bovine serum albumin (BSA, Sangon Biotech, A600903) passed  
622 through a 40 $\mu$ m cell strainer (Falcon), then centrifuged. Dead cells were removed by  
623 magnetic bead purification (Miltenyi Biotech) according to the manufacturer's protocol  
624 before scRNA-seq was performed. Cells were resuspended with cell resuspension  
625 buffer at a viable cell concentration of 1,000 cells/ $\mu$ l.

626

627 **Single-cell RNA-seq with DNBelab C4 system**

628 The DNBelab C Series Single-Cell Library Prep Set (MGI) was utilized as previously  
629 described (Liu et al., 2019) for single-cell RNA-seq library preparation. In brief, the  
630 single-cell suspensions were converted to barcoded scRNA-seq libraries through  
631 steps including droplet encapsulation, emulsion breakage, mRNA captured bead  
632 collection, reverse transcription, cDNA amplification and purification. Indexed  
633 sequencing libraries were constructed according to the manufacturer's protocol. The  
634 sequencing libraries were quantified by Qubit™ ssDNA Assay Kit (Thermo Fisher  
635 Scientific). The sequencing libraries were sequenced by the DIPSEQ T1 sequencer at  
636 China National GeneBank (CNGB). The read structure was paired-end with Read 1,  
637 covering 30 bases inclusive of 10-bp cell barcode 1, 10-bp cell barcode 2 and 10-bp  
638 unique molecular identifier (UMI), and Read 2 containing 100 bases of transcript  
639 sequence, 10-bp sample index.

640

641 **QUANTIFICATION AND STATISTICAL ANALYSIS**

642 **Single-cell RNA-seq data processing. (Alignment, Barcode Assignment, and**

643 **UMI Counting)**

644 The raw FASTQ files were transformed using custom Perl scripts into Cell  
645 Ranger-specific FASTQ files. These FASTQ files were then processed individually  
646 using a modified version of Cell Ranger count pipeline, which made use of the STAR  
647 software(v2.5.3) (Dobin et al., 2013) to align cDNA reads to the GRCh38.p5 human  
648 reference genome. Aligned reads were then filtered for valid cell barcodes and UMIs  
649 to generate gene-cell matrices for downstream analysis.

650

651 **Detection of SARS-CoV-2 transcript**

652 The genome of SARS-CoV-2 was downloaded from NCBI  
653 (<https://www.ncbi.nlm.nih.gov/>) with the accession number NC\_045512.2. The raw  
654 sequencing reads were then aligned to the genome by STAR (v2.5.3) (Dobin et al.,  
655 2013) and Bowtie2 (Langmead and Salzberg, 2012) using a modified annotation GTF  
656 file.

657

658 **Unsupervised clustering**

659 Cell clustering was performed by Seurat (v3.1) R toolkit (Butler et al., 2018)  
660 (<https://github.com/satijalab/seurat>). Genes expressed in less than 3 cells were  
661 filtered out and cells with less than 300 or more than 6000 genes detected were  
662 excluded. In order to deal with the batch effect, the “NormalizeData” and  
663 “FindVariableGene” function were performed respectively for each sample (n=23).  
664 After that, these 23 batches were integrated together using “FindIntergrationAnchors”  
665 and “IntegrateData” function with dims parameter set to 20. Then, the integrated  
666 dataset was scaled and PCA was calculated. The first 20 PCs were used to construct  
667 a SNN network and a graph-based clustering approach, louvain algorithm, was  
668 applied to identify cell clusters with the resolution set to 1. Finally, UMAP was applied  
669 to visualize the clustering result in 2D space. To further regress out the influence of  
670 blood cells, we excluded this cluster of cells as well as 10 hemoglobin genes in the  
671 expression matrix (*HBA1*,*HBA2*, *HBB*, *HBG1*, *HBG2*, *HBQ1*, *HBD*, *HBM*, *HBE1* and  
672 *HBZ*), and performed clustering again using the same method described above.

673

#### 674 **Cluster marker analysis and cell type annotation**

675 To annotate each cluster to a specific immune cell type, we selected some classic  
676 markers for immune cells and used violin plots (Figure 1D) and UMAP feature plots  
677 (Figure S1) to annotate cell types. The following genes were used for cell type  
678 annotation: CD3G, CD4, CD8A, CD8B (T cells) ; KLRF1,XCL1 (NKs) ; MS4A1 (B  
679 cells) ; CD27 (Memory B cells) IGHG1, MZB1 (Plasma cells) ; CD68 (Monocytes) ;

680 CD1C, LYZ (DCs) ; MKI67, TOP2A (Cycling cells) ; GZMA (Cytotoxic CD8<sup>+</sup> T cells /  
 681 NKs) ; CCR7, SELL (Naive T cells) ; PPBP (Megakaryocytes) ; CD34 (Stem cells).

682

683 **Differential expressed genes (DEGs) analysis and GO enrichment**

684 We performed DEG analysis using the “FindMarkers” function in Seurat R package.  
 685 The cell populations we wanted to compare were input as ident.1 and ident.2,  
 686 respectively. The Fold change of the mean expression level of genes between the  
 687 selected cell populations were calculated. To find the function of upregulated genes  
 688 (adjusted P <0.01, Foldchange>2), we used the function compareCluster  
 689 (fun="enrichGO", pvalueCutoff=0.1, pAdjustMethod="BH",  
 690 OrgDb=org.Hs.eg.db,ontBP") of ChIPseeker R package (v.1.22.1) (Yu et al., 2015).

691

692 **Identifying time dependent transcriptional program in COVID-19 patients**

693 We used Mfuzz (Kumar and M, 2007) to identify time dependent transcriptional  
 694 program in COVID-19 patients. The sample from COVID-19 patients were grouped  
 695 according to the disease progression stage (**Table S3**). First, the average expression  
 696 of each gene was calculated for each stage. Next, we add 0.000001 for every gene to  
 697 avoid 0 in the expression matrix which was not acceptable for Mfuzz. Then, the  
 698 “filter.std(min.std=0)”, “standardize()” and “mestimate()” functions were performed for  
 699 preprocessing according to the tutorial. After that, we clustered the genes into 6

700 different expression programs (**Figure 3D**). For the GO analysis of the 6 programs,  
701 we first excluded genes with the maximum expression less than 1. Only GO terms  
702 with adjusted P value  $\leq 0.05$  were shown in the figure (**Figure 3E**).

703

704 **Box plot**

705 All of the box plots in this paper were performed using “ggboxplot()” function in ggpubr  
706 R package. Each point represents for one sample. The sample number of each group  
707 were as follow: Healthy donors (Ctrl) (n=3), COV-19 patients (COV) (n=16), IAV  
708 patients (IAV) (n=4). The horizontal line within each box represents the median, the  
709 top and bottom of each box indicate the 75th and 25th percentile. Student's t test was  
710 applied to test the significance of the difference using “stat\_compare\_means()”  
711 function.

712

713 **Quantification and statistical analysis**

714 Statistical analysis was performed using R (version 3.6.1). Wilcoxon rank-sum test,  
715 Student's t-test were used in this study. \*  $p < 0.05$ , \*\* $p < 0.01$ , \*\*\* $p < 0.001$ .

716

717 **Table S1. Clinical data of the enrolled subjects, Related to Figure 1.**

718 **Table S2. Clinical laboratory test, Related to Figure 2.**

719 **Table S3. Disease progression stage information, Related to Figure 3.**

720

721 **REFERENCES**

722

- 723 Butler, A., Hoffman, P., Smibert, P., Papalexi, E., and Satija, R. (2018). Integrating single-cell  
 724 transcriptomic data across different conditions, technologies, and species. *Nat. Biotechnol.* **36**,  
 725 411-420.
- 726 Chen, N., Zhou, M., Dong, X., Qu, J., Gong, F., Han, Y., Qiu, Y., Wang, J., Liu, Y., Wei, Y., *et al.* (2020).  
 727 Epidemiological and clinical characteristics of 99 cases of 2019 novel coronavirus pneumonia in  
 728 Wuhan, China: a descriptive study. *Lancet* **395**, 507-513.
- 729 Desai, P., Tahiliani, V., Hutchinson, T.E., Dastmalchi, F., Stanfield, J., Abboud, G., Thomas, P.G., Ware,  
 730 C.F., Song, J., Croft, M., and Salek-Ardakani, S. (2018). The TNF superfamily molecule LIGHT  
 731 promotes the generation of circulating and lung-resident memory CD8 T cells following an acute  
 732 respiratory virus infection. *J. Immunol.* **200**, 2894-2904.
- 733 Dobin, A., Davis, C.A., Schlesinger, F., Drenkow, J., Zaleski, C., Jha, S., Batut, P., Chaisson, M., and  
 734 Gingeras, T.R. (2013). STAR: ultrafast universal RNA-seq aligner. *Bioinformatics* **29**, 15-21.
- 735 Elmore, S. (2007). Apoptosis: a review of programmed cell death. *Toxicol. Pathol.* **35**, 495-516.
- 736 Gan, H., Hao, Q., Idell, S., and Tang, H. (2015). Transcription factor Runx3 is induced by influenza A  
 737 virus and double-strand RNA and mediates airway epithelial cell apoptosis. *Sci. Rep.* **5**, 17916.
- 738 Gao, G.F. (2018). From "A"IV to "Z"IKV: attacks from emerging and re-emerging pathogens. *Cell* **172**,  
 739 1157-1159.
- 740 Huang, C., Wang, Y., Li, X., Ren, L., Zhao, J., Hu, Y., Zhang, L., Fan, G., Xu, J., Gu, X., *et al.* (2020). Clinical  
 741 features of patients infected with 2019 novel coronavirus in Wuhan, China. *Lancet* **395**, 497-506.
- 742 Huang, F., Guo, J., Zou, Z., Liu, J., Cao, B., Zhang, S., Li, H., Wang, W., Sheng, M., Liu, S., *et al.* (2014).  
 743 Angiotensin II plasma levels are linked to disease severity and predict fatal outcomes in  
 744 H7N9-infected patients. *Nat. Commun.* **5**, 3595.
- 745 Jeong, S.I., Kim, J.W., Ko, K.P., Ryu, B.K., Lee, M.G., Kim, H.J., and Chi, S.G. (2018). XAF1 forms a positive  
 746 feedback loop with IRF-1 to drive apoptotic stress response and suppress tumorigenesis. *Cell*

- 747 Death Dis. 9, 806.
- 748 Li, W., Moore, M.J., Vasilieva, N., Sui, J., Wong, S.K., Berne, M.A., Somasundaran, M., Sullivan, J.L.,  
749 Luzuriaga, K., Greenough, T.C., *et al.* (2003). Angiotensin-converting enzyme 2 is a functional  
750 receptor for the SARS coronavirus. Nature 426, 450-454.
- 751 Liu, W.J., Zhao, M., Liu, K., Xu, K., Wong, G., Tan, W., and Gao, G.F. (2017). T-cell immunity of SARS-CoV:  
752 Implications for vaccine development against MERS-CoV. Antiviral. Res. 137, 82-92.
- 753 Ludwig, S., and Planz, O. (2008). Influenza viruses and the NF-kappaB signaling pathway - towards a  
754 novel concept of antiviral therapy. Biol. Chem. 389, 1307-1312.
- 755 Mihara, M., Hashizume, M., Yoshida, H., Suzuki, M., and Shiina, M. (2012). IL-6/IL-6 receptor system  
756 and its role in physiological and pathological conditions. Clin. Sci. 122, 143-159.
- 757 Ochiai, K., Maienschein-Cline, M., Simonetti, G., Chen, J., Rosenthal, R., Brink, R., Chong, A.S., Klein, U.,  
758 Dinner, A.R., Singh, H., and Sciammas, R. (2013). Transcriptional regulation of germinal center B  
759 and plasma cell fates by dynamical control of IRF4. Immunity 38, 918-929.
- 760 Perng, Y.-C., and Lenschow, D.J. (2018). ISG15 in antiviral immunity and beyond. Nat. Rev. Microbiol.  
761 16, 423-439.
- 762 Raju, S., Kometani, K., Kurosaki, T., Shaw, A.S., and Egawa, T. (2018). The adaptor molecule CD2AP in  
763 CD4 T cells modulates differentiation of follicular helper T cells during chronic LCMV infection.  
764 PLoS Pathog. 14, e1007053.
- 765 Rath, P.C., and Aggarwal, B.B. (1999). TNF-induced signaling in apoptosis. J. Clin. Immunol. 19,  
766 350-364.
- 767 Rolfs, M.A., Foppa, I.M., Garg, S., Flannery, B., Brammer, L., Singleton, J.A., Burns, E., Jernigan, D.,  
768 Olsen, S.J., Bresee, J., and Reed, C. (2018). Annual estimates of the burden of seasonal influenza  
769 in the United States: A tool for strengthening influenza surveillance and preparedness. Influenza  
770 Other Respir. Viruses 12, 132-137.
- 771 Schoggins, J.W., and Rice, C.M. (2011). Interferon-stimulated genes and their antiviral effector  
772 functions. Curr. Opin. Virol. 1, 519-525.
- 773 Shaffer, A.L., Shapiro-Shelef, M., Iwakoshi, N.N., Lee, A.H., Qian, S.B., Zhao, H., Yu, X., Yang, L., Tan, B.K.,  
774 Rosenwald, A., *et al.* (2004). XBP1, downstream of Blimp-1, expands the secretory apparatus and  
775 other organelles, and increases protein synthesis in plasma cell differentiation. Immunity 21,  
776 81-93.
- 777 Shapira, S.D., Gat-Viks, I., Shum, B.O., Dricot, A., de Grace, M.M., Wu, L., Gupta, P.B., Hao, T., Silver, S.J.,  
778 Root, D.E., *et al.* (2009). A physical and regulatory map of host-influenza interactions reveals

- 779 pathways in H1N1 infection. *Cell* 139, 1255-1267.
- 780 Straszewski-Chavez, S.L., Visintin, I.P., Karassina, N., Los, G., Liston, P., Halaban, R., Fadiel, A., and Mor,  
781 G. (2007). XAF1 mediates tumor necrosis factor-alpha-induced apoptosis and X-linked inhibitor of  
782 apoptosis cleavage by acting through the mitochondrial pathway. *J. Biol. Chem.* 282,  
783 13059-13072.
- 784 Thevarajan, I., Nguyen, T.H.O., Koutsakos, M., Druce, J., Caly, L., van de Sandt, C.E., Jia, X., Nicholson, S.,  
785 Catton, M., Cowie, B., *et al.* (2020). Breadth of concomitant immune responses prior to patient  
786 recovery: a case report of non-severe COVID-19. *Nat. Med.* 26, 453-455.
- 787 Wang, C., Horby, P.W., Hayden, F.G., and Gao, G.F. (2020a). A novel coronavirus outbreak of global  
788 health concern. *Lancet* 395, 470-473.
- 789 Wang, Q., Zhang, Y., Wu, L., Niu, S., Song, C., Zhang, Z., Lu, G., Qiao, C., Hu, Y., Yuen, K.-Y., *et al.* (2020b).  
790 Structural and functional basis of SARS-CoV-2 entry by using human ACE2. *Cell* 181, 894-904  
791 e899.
- 792 Wang, Z., Yang, B., Li, Q., Wen, L., and Zhang, R. (2020c). Clinical features of 69 cases with Coronavirus  
793 Disease 2019 in Wuhan, China. *Clin. Infect. Dis.* ciaa272.
- 794 Wolf, J., Rose-John, S., and Garbers, C. (2014). Interleukin-6 and its receptors: a highly regulated and  
795 dynamic system. *Cytokine* 70, 11-20.
- 796 Wu, J.T., Leung, K., and Leung, G.M. (2020). Nowcasting and forecasting the potential domestic and  
797 international spread of the 2019-nCoV outbreak originating in Wuhan, China: a modelling study.  
798 *Lancet* 395, 689-697.
- 799 Xiong, Y., Liu, Y., Gao, L., Wang, D., Guo, M., Guo, D., Hu, W., Yang, J., Tang, Z., Zhang, Q., *et al.* (2020).  
800 Transcriptomic characteristics of bronchoalveolar lavage fluid and peripheral blood mononuclear  
801 cells in COVID-19 patients. *Emerg. Microbes. Infect.* 9, 761-770.
- 802 Xu, H., Zhong, L., Deng, J., Peng, J., Dan, H., Zeng, X., Li, T., and Chen, Q. (2020a). High expression of  
803 ACE2 receptor of 2019-nCoV on the epithelial cells of oral mucosa. *Int. J. Oral. Sci.* 12, 8.
- 804 Xu, X., Han, M., Li, T., Sun, W., Wang, D., Fu, B., Zhou, Y., Zheng, X., Yang, Y., Li, X., *et al.* (2020b).  
805 Effective treatment of severe COVID-19 patients with tocilizumab. *Proc. Natl. Acad. Sci. USA* 117,  
806 10970-10975.
- 807 Yu, G., Wang, L.G., and He, Q.Y. (2015). ChIPseeker: an R/Bioconductor package for ChIP peak  
808 annotation, comparison and visualization. *Bioinformatics* 31, 2382-2383.
- 809 Yu, X., Zhang, X., Zhao, B., Wang, J., Zhu, Z., Teng, Z., Shao, J., Shen, J., Gao, Y., Yuan, Z., and Wu, F.  
810 (2011). Intensive cytokine induction in pandemic H1N1 influenza virus infection accompanied by

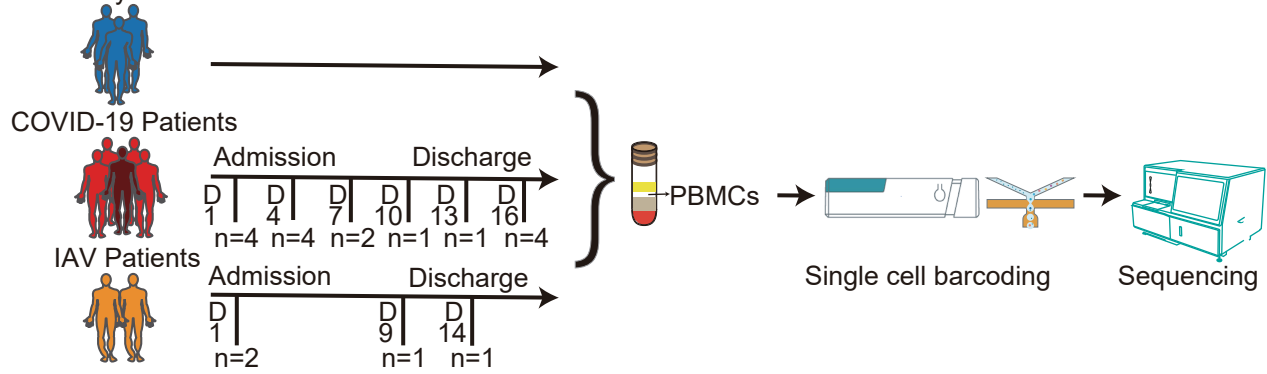
- 811 robust production of IL-10 and IL-6. PLoS ONE 6, e28680.
- 812 Zhang, F., Chen, D., Yang, W., Duan, S., and Chen, Y. (2019). Combined effects of XAF1 and TRAIL on the  
813 apoptosis of lung adenocarcinoma cells. Exp. Ther. Med. 17, 4663-4669.
- 814 Zhao, M., Zhang, H., Liu, K., Gao, G.F., and Liu, W.J. (2017). Human T-cell immunity against the  
815 emerging and re-emerging viruses. Sci. China Life Sci. 60, 1307-1316
- 816 Zhou, F., Yu, T., Du, R., Fan, G., Liu, Y., Liu, Z., Xiang, J., Wang, Y., Song, B., Gu, X., et al. (2020a). Clinical  
817 course and risk factors for mortality of adult inpatients with COVID-19 in Wuhan, China: a  
818 retrospective cohort study. Lancet 395, 1054-1062.
- 819 Zhou, P., Yang, X.-L., Wang, X.-G., Hu, B., Zhang, L., Zhang, W., Si, H.-R., Zhu, Y., Li, B., Huang, C.-L., et al.  
820 (2020b). Discovery of a novel coronavirus associated with the recent pneumonia outbreak in  
821 humans and its potential bat origin. bioRxiv, 2020.2001.2022.914952.
- 822 Zhou, Y., Fu, B., Zheng, X., Wang, D., Zhao, C., Qi, Y., Sun, R., Tian, Z., Xu, X., and Wei, H. (2020c).  
823 Pathogenic T cells and inflammatory monocytes incite inflammatory storm in severe COVID-19  
824 patients. National Science Review 7, 998-1002.
- 825 Zou, B., Chim, C.S., Pang, R., Zeng, H., Dai, Y., Zhang, R., Lam, C.S., Tan, V.P., Hung, I.F., Lan, H.Y., and  
826 Wong, B.C. (2012). XIAP-associated factor 1 (XAF1), a novel target of p53, enhances  
827 p53-mediated apoptosis via post-translational modification. Mol. Carcinog. 51, 422-432.
- 828

**Highlights:**

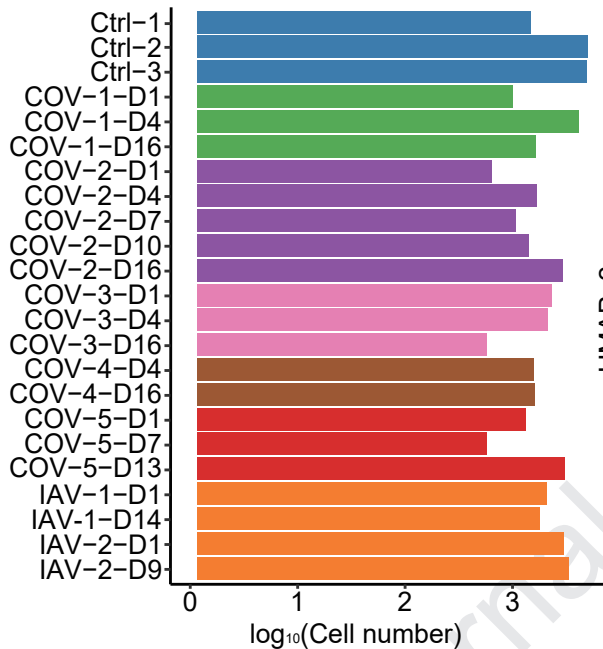
- We generated a single-cell atlas of PBMCs in both COVID-19 and influenza patients.
- Plasma cells increase significantly in both COVID-19 and influenza patients.
- COVID-19 is featured with XAF1-, TNF- and FAS-induced T cell apoptosis.
- Distinct pathways activate in COVID-19 (STAT1/IRF3) vs. influenza (STAT3/NF $\kappa$ B) patients.

**In Brief**

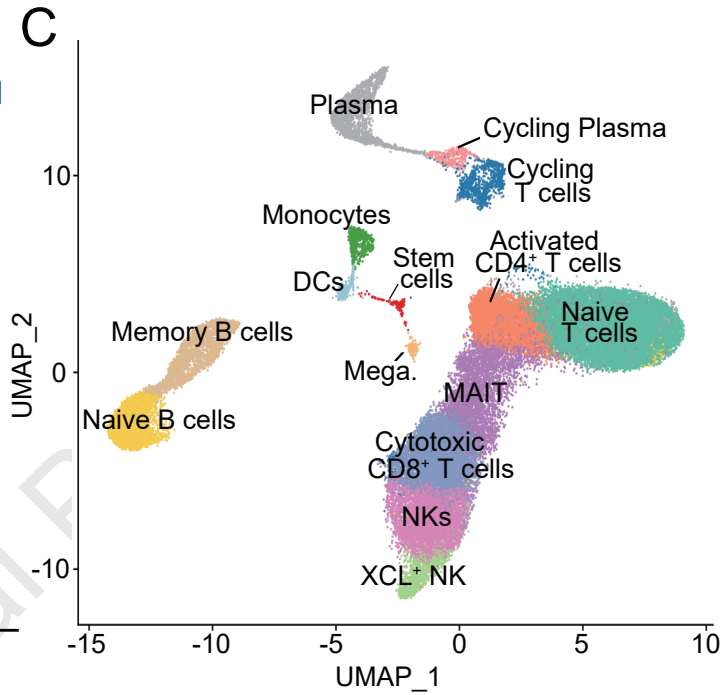
COVID-19 and influenza are both respiratory infections with cytokine release syndrome. Zhu et al. use single-cell RNA sequencing of longitudinally collected PBMCs in both patients to reveal distinct immune response landscapes of the two diseases and identify virus-specific cell composition and immune response pathways.



B



C



D

